Desalination and Water Treatment
www.deswater.com
doi: 10.5004/dwt.2023.29951

312 (2023) 177–186
November

Study on the process and mechanism of chloride ion adsorption by ultra-high lime aluminum method

Pengyu Zhang[a], Limin Sun[b], Wenyang Li[a], Haomeng Guo[a], Ruian Gao[c], Yong Guan[d,*], Liming Feng[a,*]

[a]*Shandong Jianzhu University, No. 100 of Feng Ming Road, Jinan 250000, China, emails: flm@sdjzu.edu.cn (L.M. Feng), 1711547738@qq.com (P.Y. Zhang), 864634812@qq.com (W.Y. Li), 1346464229@qq.com (H.M. Guo)*
[b]*Shanghai Institute of Space Power-Sources, 200245 Shanghai, China, email: 2177816841@qq.com*
[c]*Weifang Guoyi Aluminum Co., Ltd., email: lgjyf2019@163.com*
[d]*Institute of Metal Research, Chinese Academy of Sciences, Shenyang 110016, China, email: yguan@imr.ac.cn*

Received 13 March 2023; Accepted 7 September 2023

ABSTRACT

The ultra-high lime aluminum method (UHLA) is a method that can effectively adsorb chloride ions in a solution. Calcium oxide (CaO) and sodium aluminate ($NaAlO_2$) were mixed and added to the sodium chloride solution. After the reaction lasted for some time, the content of chloride ions in the solution was significantly reduced. Through the experiment of chloride ion adsorption, it was found that when the mass ratio of calcium oxide to sodium aluminate was m($NaAlO_2$):m(CaO) = 1:2.5, the reaction temperature was 25°C, and the stirring time was 60 min, the adsorption effect on chloride ion was the best. The adsorption rate can reach 93.3% in a 100 mg/L sodium chloride solution. With the increased sodium chloride concentration, the time required to reach adsorption equilibrium becomes longer. In a 2,000 mg/L sodium chloride solution, this method's unit adsorption mass of chloride ion can reach 63.5 mg/g. Through SEM and XRD analysis, calcium oxide and sodium aluminate react in solution to form $Ca_4Al_2(OH)_{14}$ with a layered structure. The OH^- between the layers can exchange with external chloride ions. After $Ca_4Al_2(OH)_{14}$ adsorbs chloride ions, the product is Friedel's salt ($Ca_4Al_2Cl_2(OH)_{12}$) with the same layered structure.

Keywords: Chlorine; Friedel's salt; Alyered structure; Ion exchange; Aluminum

1. Introduction

Chloride ion is one of nature's most stable forms of chlorine [1]. If chlorine ion exists in large quantities in water, it is not conducive to the growth of aquatic plants and animals, harming the ecological environment. Drinking too much water containing excessive chloride ions harms human health [2–6]. The chloride ion is a common corrosive anion. Its significant presence will cause irreversible corrosion damage to industrial equipment. For example, pipelines working in the marine environment are seriously corroded under the long-term influence of chloride ions in seawater and the marine atmosphere [7–10]. In addition, the water quality standard for sewage discharged into urban sewers (GB/T 31962-2015) stipulates that the chloride ion concentration in sewage discharge shall not exceed 500 mg/L, and even some regulations require that the discharge concentration be less than 400 mg/L [11]. It is essential to control the lowest concentration of chloride ions in sewage. There are also many methods to remove chloride ions in industry. The main methods for removing high chloride ions are the precipitation salt method [12–15], the membrane separation method [16], the evaporation concentration method [17], the ion exchange method, and

* Corresponding author.

so on [18–23]. Generally, chloride ions can form soluble salt with most metal ions, and silver ions can react with chloride ions to form a precipitate. However, it is expensive, so removing chloride ions by precipitation is challenging. Membrane separation can remove chloride ions, but the removal efficiency will decrease when the concentration is high. At the same time, other impurities in the wastewater may damage the membrane module. UHLA can react with chloride ions in water to produce one or more insoluble calcium and aluminum chloride compounds precipitated to remove chloride ions. The method has the advantages of low cost, fast response, low energy consumption, simple operation, and has good practical application value. In addition, the resulting sediments can also be used to adsorb other heavy metal ions. Many scientific researchers have studied the law of chloride ion adsorption at UHLA.

For example, Abdel-Wahab and Batchelor [24,25] conducted equilibrium and kinetic experiments to evaluate the chloride removal in circulating cooling water by the ultra-high lime aluminum process and characterized the equilibrium conditions of calcium aluminate chloride precipitation. The optimum pH for maximum chloride removal efficiency was 12 ± 0.2; Xin et al. [26] developed a two-stage desalination process to realize zero liquid discharge of flue gas desulfurization wastewater and convert chloride into precipitation. When the calcium-aluminum molar ratio was 3.0, the chloride ion removal effect was the best. It was reported in the literature that this precipitate was exchanged with chloride ions to form another precipitate, namely Friedel's salt [27]. Friedel's salt is a layered bimetallic hydroxide (LDH) and an excellent adsorbent that can adsorb heavy metal ions and other harmful substances in wastewater, such as chromium, cadmium, arsenic, and other elements. For example, Dai et al. [28] focused on the experimental study of the adsorption and fixation of Cr^{6+} by Friedel's salt in an aqueous solution. Li et al. [29] studied the adsorption and removal of arsenic by Friedel's salt in an aqueous solution.

Researchers have extensively researched Friedel's salt's adsorption of harmful ions, which has a good application prospect. After searching for relevant information about this method, found that their focus is on the amount of adsorption that can be achieved under what conditions. However, this method's specific adsorption mode and characterization could be much better. Even the description of the whole adsorption process is minimal. This paper aims to study the optimal adsorption formula and influencing factors and to characterize before and after adsorption. The precipitate from the calcium oxide and sodium aluminate reactions in deionized water was characterized. Whether the precipitate had an adsorption effect on chloride ions was explored, compared with a simple mixed addition of calcium oxide and sodium aluminate, and their adsorption mechanisms were further discussed.

On this basis, the influence of temperature, time, and pH on the adsorption of chloride ions by the ultra-high lime method was studied, and the adsorption of chloride ions by prefabricated precipitates was studied. XRD, SEM, and FTIR were used to characterize before and after adsorption. The ultra-high lime method's adsorption process of chloride ions was analyzed, and the adsorption mechanism was discussed in depth.

2. Materials and methods

2.1. Materials

Sodium (AR) and sodium aluminate (CP) was purchased from Sinopharm Chemical Reagent Co., Ltd. Calcium oxide (AR) was purchased from Shanghai McLean Biochemical Technology Co., Ltd. Silver nitrate (AR) and potassium chromate (AR) were purchased from the Tianjin Damao Chemical Reagent Factory, and deionized water (H_2O) was self-made in the laboratory.

2.2. Preparation and feeding method of calcium aluminum precipitation

In order to discuss the adsorption effect and adsorption stage of chloride ions by the ultra-high lime method, two groups of experiments will be set up to study whether the precipitate formed by calcium oxide and sodium aluminate in water has the main adsorption effect on chloride ions or whether calcium oxide and sodium aluminate adsorb chloride ions in the process of forming a precipitate.

CaO and $NaAlO_2$ were mixed according to the mass ratio in Table 1, and the mixture was marked as Mix-A, then added to a 200 mL sodium chloride solution with a 300 mg/L concentration. Mix-A was added to the sodium chloride solution, and the precipitate produced after the reaction was labeled as Sed-C, as shown in Fig. 1a. In the process, the working speed of the centrifuge r = 10,000 rpm, the working time t = 120 s, and the rotating speed of the magnetic stirrer r = 400 rpm. The feed ratio, reaction time, and temperature effects on chloride ion adsorption were studied.

CaO was added to deionized water at 25°C. Then a certain amount of $NaAlO_2$ was added in the ratio of $m(NaAlO_2):m(CaO)$ = 1:2.5. After a reaction period, a precipitated product was obtained and labeled as Sed-B. Sed-B was dried in an oven (50°C) for 3 h, then taken out and washed twice with distilled water to remove residual impurities; it was baked in an oven at 50°C for 3 h, dried and ground to obtain Sed-B white powder. A specific mass of Sed-B powder was added to the sodium chloride solution, and the precipitate after the reaction was labeled as Sed-D, as shown in Fig. 1b. The adsorption efficiency and adsorption capacity were measured at different reaction times. The experiment was strictly controlled with the variables—centrifuge working speed r = 10,000 rpm, working time t = 120 s, heating magnetic stirrer speed r = 400 rpm.

Table 1
Mass ratio of $NaAlO_2$ and CaO

$m(NaAlO_2):m(CaO)$	Actual added mass
1:1	0.3:0.3 g
1:1.3	0.3:0.39 g
1:1.5	0.3:0.45 g
1:2	0.3:0.6 g
1:2.5	0.3:0.75 g
1:3	0.3:0.9 g

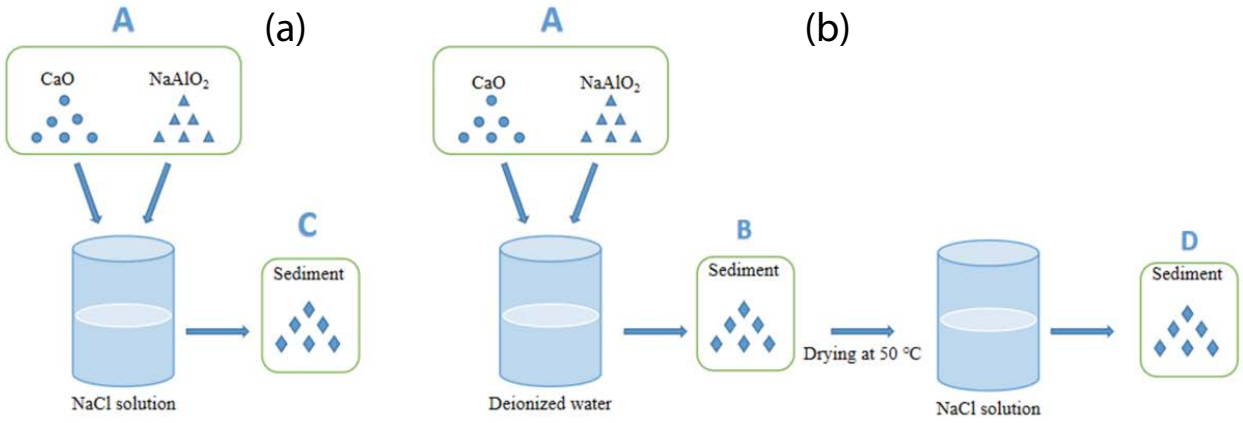

Fig. 1. Schematic diagram of feeding mode (The Mix-A stands for the mixture of CaO and $NaAlO_2$; Sed-B represents the precipitate after adding Mix-A to deionized water for reaction; Sed-C represents the precipitate after the reaction of Mix-A in sodium chloride solution; Sed-D represents the precipitate after adding Sed-B to sodium chloride solution for reaction.).

2.3. Structural characterization before and after adsorption

X-ray diffraction analysis (XRD) was used to detect the crystal structure of the sample, and PANalytical X'Pert PROX diffractometer was used. with Cu K-α radiation (λ = 1.54 Å) at 40 kV and 40 mA. A scanning rate of 0.02°/s was applied to record the patterns in the 2θ angle range from 5° to 90°.

Use a Thermo Scientific Nicolet iS20 infrared spectrometer to measure the infrared absorption of the sample. Take 1–2 mg of sample and potassium bromide powder, mix them evenly, put them into the mold, and press them into pieces on the tablet press for testing. Scanning range: 4,000–400 cm^{-1}, the number of scans was 32, and the resolution was 4 cm^{-1}.

The gold spraying treatment is carried out on the surface of the sample. The structure and morphology of the adsorbent before and after the reaction were studied by scanning electron microscope (SEM) Thermo Scientific Apreo 2C, and the types and contents of elements were analyzed by EDS.

2.4. Chloride ion detection method

Chloride ion concentration was measured by the national standard GB/T11896-89 (Determination of Chloride in Water Quality by Silver Nitrate Titration). Using potassium chromate as an indication, a certain amount of potassium chromate was added to the solution under test, and then a predetermined concentration of silver nitrate solution was steadily added until the solution under test turned brick red, precipitated, and stopped. signifies the achievement of the titration endpoint. The chloride content *C* at equilibrium is shown in Eq. (1). The determination was repeated three times for each sample, and the average value was taken.

$$C = \frac{M\left(V_2 - V_1\right)\times 35.5}{V}\times 1000 \quad (1)$$

where V_1 is the amount of silver nitrate standard solution consumed by deionized water (mL), V_2 is the amount of silver nitrate standard solution consumed by the sample (mL), M is the concentration of silver nitrate standard solution (mol/L), V is the sample volume (mL), 35.45 is Cl^- relative atomic mass (g/mol).

The removal rate of chloride ions is shown in Eq. (2):

$$\eta = \frac{\left(C_0 - C\right)}{C_0}\times 1000 \quad (2)$$

where C_0 is the initial mass concentration of chloride ion (mg/L), C is the mass concentration of chloride ion at equilibrium (mg/L).

The unit adsorption Q_e (mg/g) when the chloride ion reaches equilibrium is shown in Eq. (3).

$$Q_e = \frac{\left(C_0 - C_e\right)V}{m} \quad (3)$$

The unit adsorption Q_t (mg/g) of chloride ion at time t is shown in Eq. (4).

$$Q_t = \frac{\left(C_0 - C_t\right)V}{m} \quad (4)$$

where C_0 is the initial mass concentration of chloride ion (mg/L), C_e is the concentration of chloride ion at equilibrium, C_t is the mass concentration of chloride ion at time t (mg/L), V volume of salt solution (L), m is the addition amount of adsorbent (g).

3. Results and discussion

3.1. Structural characterization before and after adsorption

3.1.1. SEM/EDS analysis of precipitates before and after adsorption

The SEM images of the precipitates before and after adsorption are shown in Fig. 2. The morphology of Sed-B generated by adding Mix-A to deionized water without adsorption of chloride ions is shown in Fig. 2a. From the

image, it can be seen that the structure of the reaction product is formed by layered stacking, which conforms to the morphological characteristics of $Ca_4Al_2(OH)_{14}$ with layered structure [30,31]. Sed-B was added to a sodium chloride solution after drying at 50°C, and the shape of Sed-D that resulted from the adsorption of chloride ions is depicted in Fig. 2b. The flakes' density and visible structural elements can be viewed. Some of them were 1–3 um-sized flat hexagons. This shape matched Friedel's salt's physical traits and was typical of LDH structures [32–34], As shown in Fig. 2b, the part marked by the red ellipse. The Sed-C created by mixing Mix-A with sodium chloride solution and adsorbing chloride ions is depicted in Fig. 2c. The precipitates are primarily layered as seen in the image, while some are flat hexagons and clusters that are more concentrated than in Fig. 2b.

The energy spectrum scan before and after adsorption shows that, as shown in Fig. 3, there was no spectrum line for chlorine in Sed-B. However, there was more spectrum line of chlorine element in Sed-C, indicating that calcium oxide and sodium aluminate can fix chloride ion in the reaction sediment in sodium chloride solution.

3.1.2. XRD analysis of precipitates before and after adsorption

As shown in Fig. 4a, through XRD pattern analysis, the main components of the Sed-B are $Ca_3Al_2(OH)_{12}$, $Ca_4Al_2(OH)_{14}$ and $Ca(OH)_2$. The prominent characteristic peaks in Sed-C and Sed-D all appear at 11.205°, 23.317°, and 30.957°, and the corresponding crystal planes are (006), (114), (222), which are consistent with the patterns of Friedel's salt match very well [35–37]. This indicates that Friedel salts exist in both Sed-C and Sed-D. According to the XRD pattern analysis, $Ca_4Al_2Cl_2(OH)_{12}$, $Ca_3Al_2(OH)_{12}$, $Ca_4Al_2(OH)_{14}$, and $Ca(OH)_2$ are the essential components of Sed-C and Sed-D. Therefore, Mix-A and Sed-B can adsorb chloride ions in a sodium chloride solution to form Friedel's salt. Compared with Fig. 4a, the diffraction peak height in Sed-C and Sed-D is enhanced, indicating that the crystallinity is increased. The low angle diffraction peak moves to the left by 0.522°. According to the calculation of the Bragg equation, the layer spacing 006 increases from 7.545–7.834 Å, which is very consistent with the layer spacing of 7.81 Å of Friedel's salt reported in the literature [28] (JCPDS No 78-1219), which is sufficient to indicate that a specific inter-layer structure may undergo ion exchange to form Friedel's salt.

3.1.3. FTIR of the precipitate before and after adsorption

Fig. 4b shows the changes in FTIR functional groups before and after adsorption. The position of 3,544 cm^{-1} is the stretching vibration peak of OH. After adsorption, the peak moves to 3,505 cm^{-1}, and intensity is significantly weakened, possibly due to the insertion of chloride ions into the inter-layer structure and the OH exchange between the layers. The stretching vibration peak of OH is reflected by the

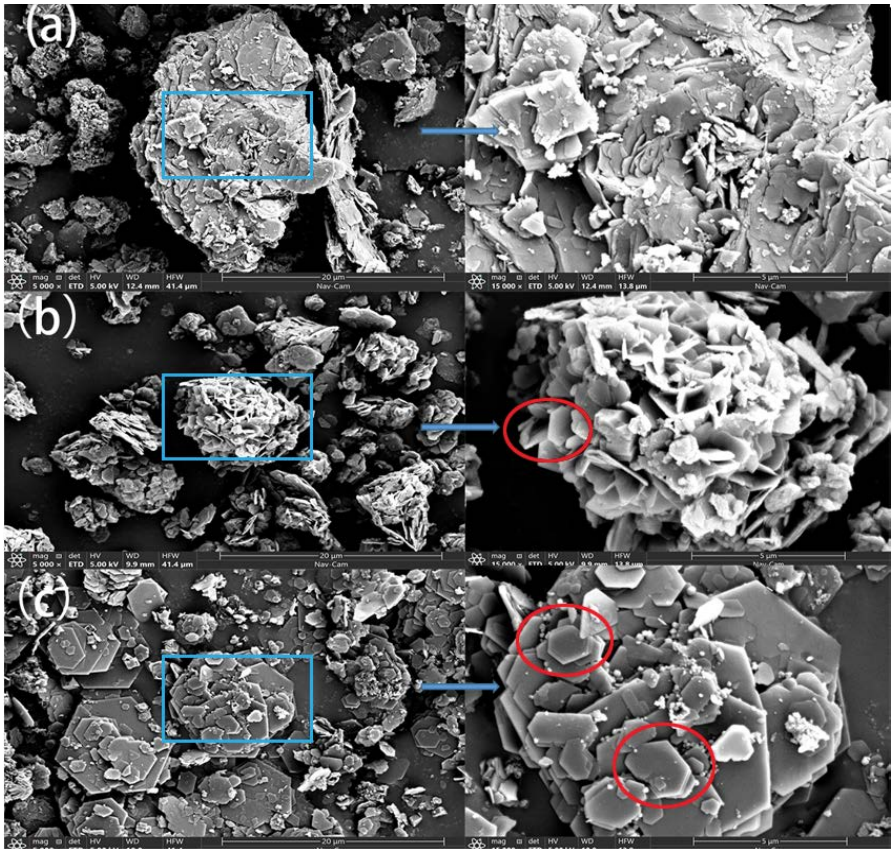

Fig. 2. SEM images before and after adsorption. SEM morphology of (a) Sed-B, (b) Sed-D and (c) Sed-C.

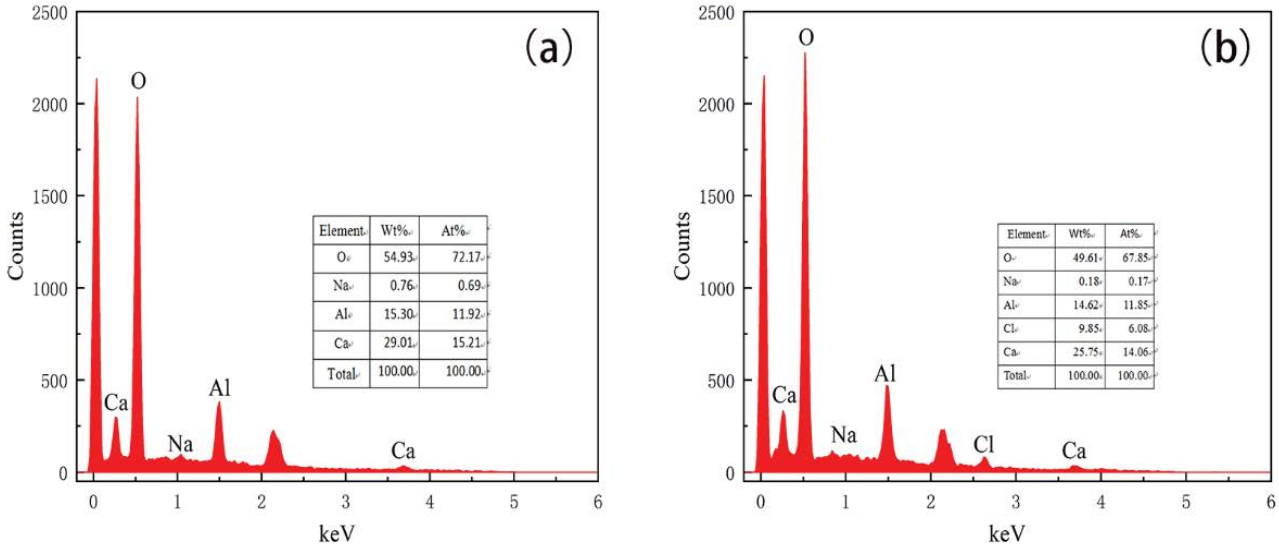

Fig. 3. EDS of Sed-B (a) and Sed-C (b).

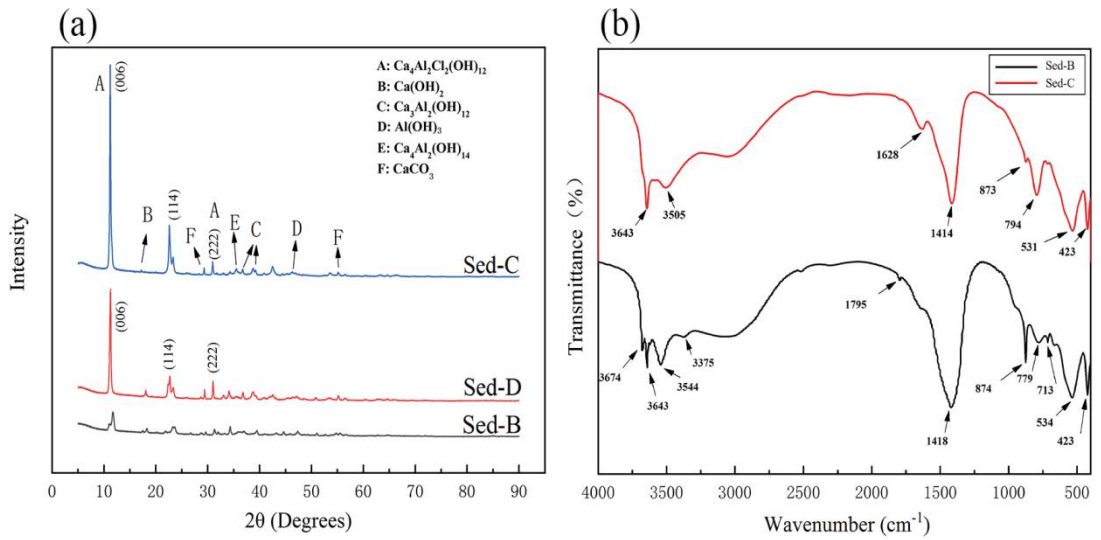

Fig. 4. XRD of Sed-B/Sed-D/Sed-C (a) and FTIR of Sed-B/Sed-C (b).

overlapping bands of 3,643 and 3,505 cm^{-1} [38]. The peak of 1,628 cm^{-1} after adsorption is more than before, which may be caused by the bending vibration of water molecules H–O–H in the inter-layer of Friedel's salt formed after adsorption. The peaks at 1,418 cm^{-1} before and 1,414 cm^{-1} after adsorption are due to CO_3^{2-}, indicating that a small amount of CO_2 in the air is also involved in the reaction process [39]. The 531 and 794.14 cm^{-1} peaks after adsorption are due to the stretching and bending vibration of Al–OH [21].

3.2. Univariate analysis

3.2.1. Effect of reaction time on chloride ion adsorption efficiency

Set the test conditions to be consistent (take 200 mL of sodium chloride solution; initial pH = 7, t = 25°C; the concentration of sodium chloride is 300 mg/L, m(NaCl):m($NaAlO_2$):m(CaO) = 1:6.5:16.25). The experimental results are shown in Fig. 5a when the Mix-A is added to the sodium chloride solution. $NaAlO_2$ and CaO will react with chloride ions continuously with increased stirring time. At first, the removal rate of chloride ions will increase with the extension of stirring. When the stirring time reaches 60 min, the adsorption efficiency and unit adsorption mass of chloride ions reach their maximum, which are 80.0% and 20.81 mg/g, respectively, With the continuous extension of the stirring time, the adsorption efficiency and unit adsorption mass of chloride ions decreased slightly.

When 1.365 g of Sed-B is added to the sodium chloride solution, as shown in Fig. 5b, the adsorption rate and unit adsorption capacity also gradually increase with the extension of the reaction time. After 60 min of reaction, the adsorption efficiency is only 16.67% and the unit adsorption

capacity is 4.45 mg/g. Compared with Mix-A, Sed-B has a poor adsorption effect. Therefore, the adsorption effect of Mix-A is much better than Sed-B's.

3.2.2. Effect of mass ratio of $NaAlO_2$ to CaO on chloride ion removal efficiency

Set the same experimental conditions (take 200 mL of sodium chloride solution, initial pH = 7, T = 25°C, stirring time = 60 min, sodium chloride concentration is 300 mg/L, m(NaCl):m($NaAlO_2$) = 1: 6.5). The experimental results are shown in Fig. 6a. With the gradual increase of CaO in the proportion, it can be found that the adsorption efficiency of chloride ions and the unit adsorption capacity are increased until m($NaAlO_2$):m(CaO) is 1:2.5. The adsorption efficiency and unit adsorption mass reached their maximum, which are 70.45% and 22.85 mg/g, respectively. The maximum unit adsorption mass was 22.85 mg/g, and the adsorption efficiency decreased slightly when the ratio of CaO was increased. The optimal feeding ratio is obtained through experiments. When m($NaAlO_2$):m(CaO) reaches 1:2.5, the adsorption efficiency reaches the highest, and the capacity of chloride ions reaches saturation. Continuing to increase CaO, the adsorption efficiency of chloride ions does not increase but tends to decrease. It may be because too much CaO reacts with $NaAlO_2$. At the same time, the resulting inter-layer structure is unstable, resulting in an increase in the OH^- concentration in the external solution and a decrease in adsorption efficiency.

3.2.3. Effect of reaction temperature on chloride ion adsorption efficiency

Set the same experimental conditions (sodium chloride solution 200 mL, initial pH = 7, stirring time = 60 min, sodium chloride concentration is 300 mg/L, m(NaCl): m($NaAlO_2$):m(CaO) = 1:6.5:16.25). The experimental results are shown in Fig. 6b. The adsorption efficiency of this method fluctuates slightly due to temperature changes. When the temperature is 25°C, the removal efficiency and unit adsorption mass of chloride ions reach the highest, which are 87% and 22.62 mg/g, respectively. It can be seen that when the temperature is slightly increased,

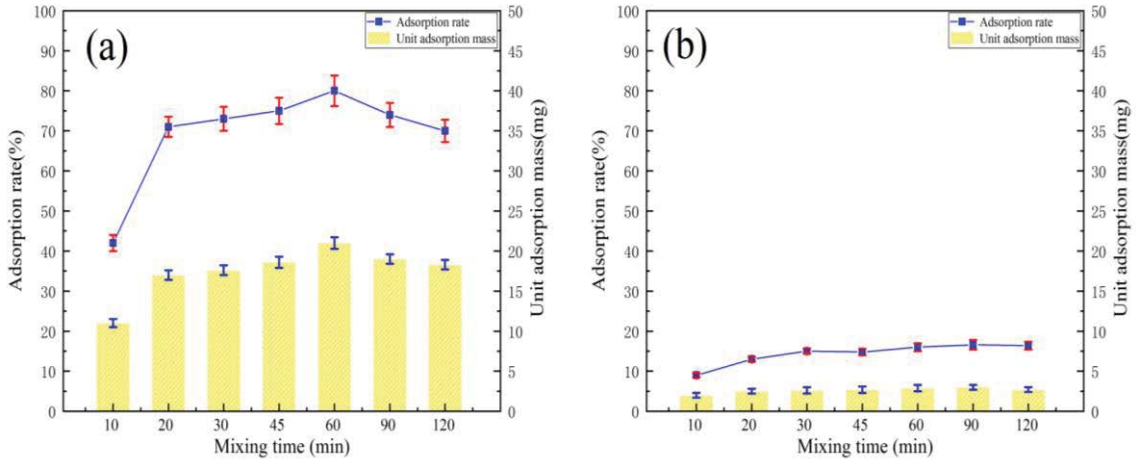

Fig. 5. Effect of reaction time on chloride ion adsorption efficiency and unit adsorption mass: Mix-A (a) and Sed-B (b) were added.

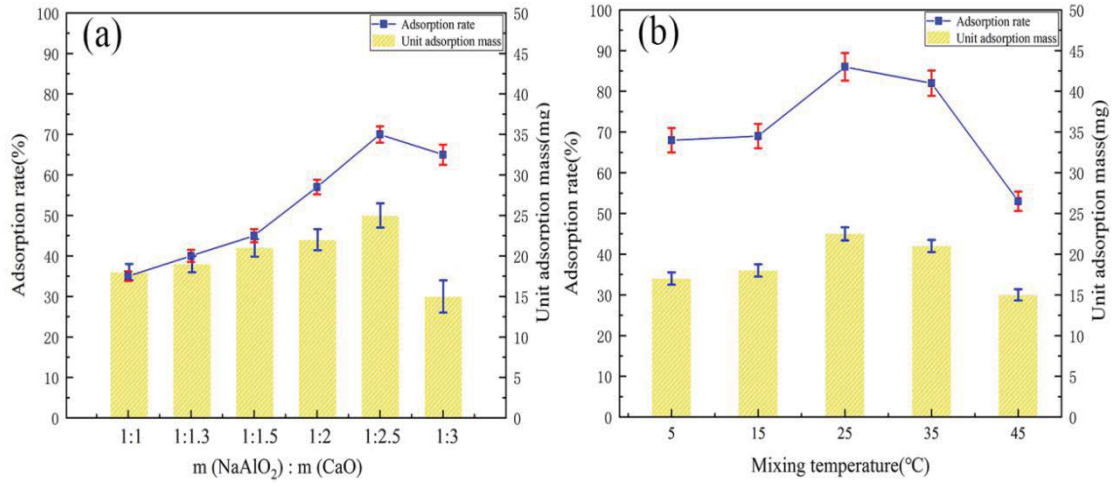

Fig. 6. Effect of mass ratio of $NaAlO_2$ to CaO (a) and reaction temperature (b) on chloride ion adsorption efficiency and unit adsorption mass.

the adsorption capacity of the method for chloride ions increases, but when the temperature is too high, it decreases. It may be that the reaction is exothermic. When the temperature exceeds a certain value, the reaction rate slows down and less substances that can adsorb chloride ions are generated, reducing the adsorption rate.

3.2.4. Effect of reaction time and sodium chloride concentration on the efficiency and unit adsorption mass of chloride ions

Set the same experimental conditions (200 mL sodium chloride solution, T = 25°C, stirring time = 60 min, m(NaCl): m($NaAlO_2$):m(CaO) = 1:6.5:16.25). The experimental results are shown in Fig. 7. When the concentration of sodium chloride solution is 100 mg/L, the adsorption efficiency of chloride ions can reach 93.3%. As the concentration of sodium chloride continues to increase, its adsorption efficiency for chloride ions decreases all the time, but the adsorption capacity per unit mass increases gradually. Because the total mass of $NaAlO_2$ and CaO added to the sodium chloride solution with different concentrations is the same. However, with the increase in the concentration of sodium chloride solution, the total concentration of chloride ions in the solution also increases, and the maximum amount of chloride ions adsorbed by the mixture of $NaAlO_2$ and CaO with the same mass is certain. Based on the same reaction time, a certain mass of adsorbent will also adsorb more chloride ions in a higher concentration of sodium chloride solution, and the unit adsorption mass will increase. When the concentration of sodium chloride solution is 2,000 mg/L, the maximum unit adsorption capacity that can be achieved is 63.50 mg/g.

3.2.5. Effect of initial pH on adsorption efficiency of UHLA for chloride ion

A certain proportion of calcium oxide and sodium chlorate was added to different concentrations of sodium chloride solution, and the reaction temperature was set at 25°C. Change the initial pH of the solution (4–12) to observe the effect of the pH change on the adsorption of chloride ion, as shown in Fig. 8. It can be seen that when the initial pH of the solution is 10, the adsorption efficiency and adsorption amount of chloride ion by UHLA reach their maximum. With the decrease of initial pH, the adsorption efficiency of Lime aluminium salt on chloride ions decreased, and the adsorption capacity decreased. When pH was greater than 10, with the increase of pH, the adsorption efficiency of Lime aluminium salt for chloride ions decreased. which might be due to acidic or neutral conditions will inhibit the formation of Freund's salt, while under strong alkaline conditions, the concentration of hydroxide ions increases, and there is a competitive relationship between chloride ions and hydroxide ions. Too many hydroxide ions will cause them to enter the Freund's salt layer to replace chloride ions and reduce the removal rate of chloride ions from the surface. Therefore, the adsorption conditions are best when the initial pH of the solution is 10.

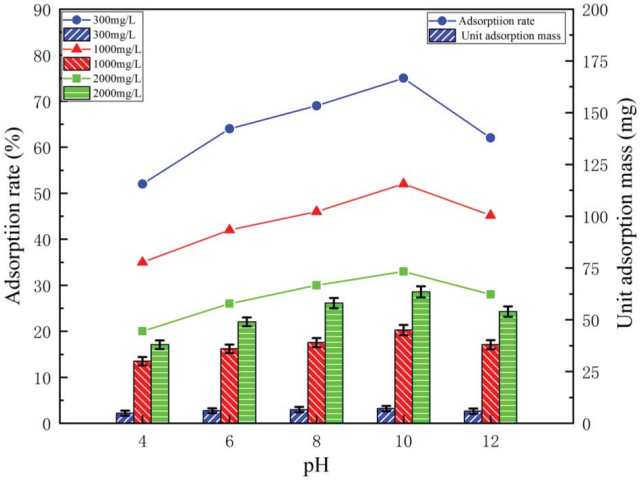

Fig. 8. Effect of different pH values on removal of chloride ion.

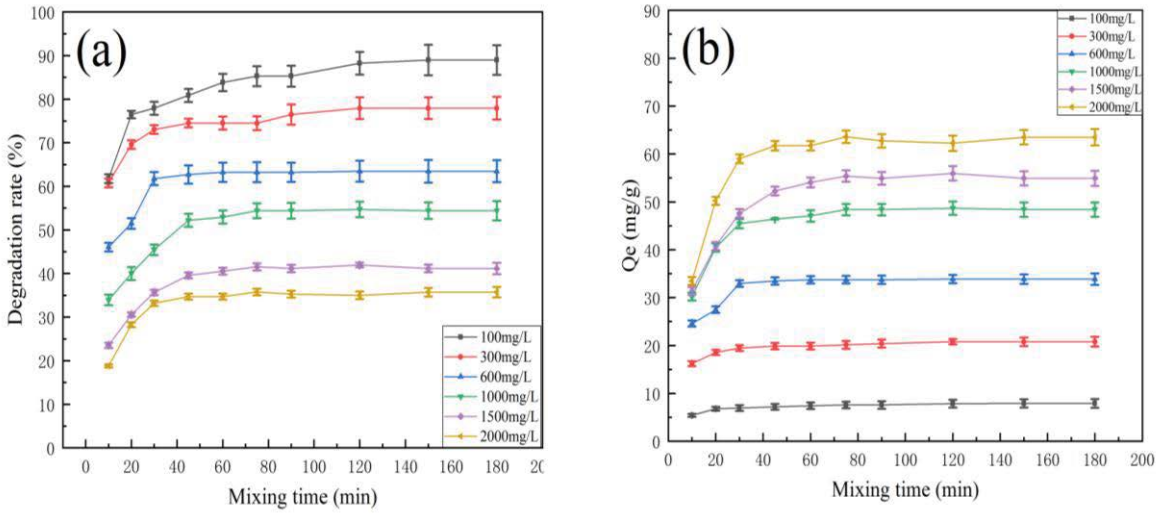

Fig. 7. Adsorption efficiency (a) and unit adsorption capacity (b) of adsorbent in different reaction time and different concentrations of sodium chloride solution.

3.3. Principle analysis

According to the principal component analysis of precipitate B in XRD patterns, as shown in Fig. 9. In aqueous solution without chloride ions, $Ca(OH)_2$ and $Al(OH)_3$ generated by the reaction continued to proceed in an aqueous environment to produce $Ca_4Al_2(OH)_{14}$, as shown in Eqs. (5–7). As the reaction continues and the generated $Ca_4Al_2(OH)_{14}$ continues to react with $Al(OH)^{4-}$ in solution to produce $Ca_3Al_2(OH)_{12}$, then the $Ca_4Al_2(OH)_{14}$ content in precipitate B will decrease as shown in Eq. (8).

$$CaO + H_2O \Rightarrow Ca(OH)_2 \quad (5)$$

$$NaAlO_2 + 2H_2O \Rightarrow Al(OH)_3 + Na^+ + OH^- \quad (6)$$

$$4Ca(OH)_2 + 2Al(OH)_3 \Rightarrow Ca_4Al_2(OH)_{14}\downarrow \quad (7)$$

$$3Ca_4Al_2(OH)_{14} + 2Al(OH)_4^- \Rightarrow 4Ca_3Al_2(OH)_{12}\downarrow + 2OH^- \quad (8)$$

In aqueous solution containing chloride ions, Sed-B showed a much poorer adsorption effect on chloride ions than Mix-A. XRD patterns indicated that the amount of $Ca_4Al_2Cl_2(OH)_{12}$ in Sed-C was less than that in Sed-D, which indicated that both Sed-B and the product of Mix-A adsorbed chloride ions were $Ca_4Al_2Cl_2(OH)_{12}$.

By reviewing the literature [8,11] it is known that $Ca_4Al_2(OH)_{14}$ is a stable structural compound with $[Ca_2Al(OH)_6]^+$ as the host layer and OH^- as the interlayer ion [30,31], both of which are maintained by hydrogen bonding, and the interlayer ion has some exchange ability, and the interlayer OH^- can be exchanged with Cl^- in solution to produce a kind of $Ca_4Al_2Cl_2(OH)_{12}$ with a less solubility product than $Ca_4Al_2(OH)_{14}$ [40]. Adding Mix-A to the water containing chloride ions with the solution, the chloride ions in the adsorbable solution of $Ca_4Al_2(OH)_{14}$ generated by the reaction transform to $Ca_4Al_2Cl_2(OH)_{12}$, and this reaction is rapid, such in Eq. (9). The poor adsorption effect of Sed-B was because after Mix-A reacted with $Ca_4Al_2(OH)_{14}$ produced in deionized water, it continued the reaction of Eq. (8).

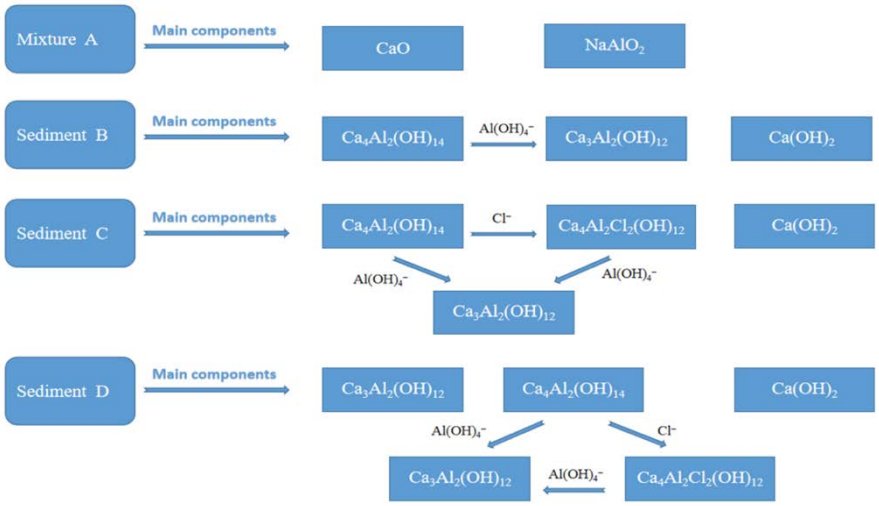

Fig. 9. Main components of each sediment.

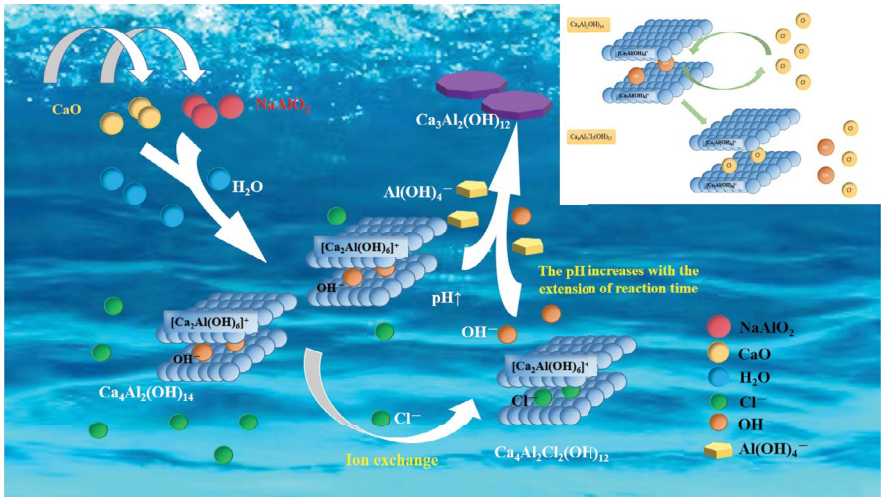

Fig. 10. Schematic diagram of $Ca_4Al_2(OH)_{14}$ adsorption mechanism of chloride ions.

Again to produce $Ca_3Al_2(OH)_{12}$ with no adsorption effect on chloride ion. The amount of $Ca_4Al_2(OH)_{14}$ in Sed-B was less, so the adsorption of chloride ions was also less effective.

When Mix-A was added to the aqueous solution containing chloride ions, the generated OH^- was gradually increased with the prolongation of reaction time, and $Ca_4Al_2Cl_2(OH)_{12}$ formed by absorbing chloride ions began to react with $Al(OH)_4$ and OH^- in the solution to desorb the adsorbed chloride ions, as shown in Eq. (10). A small amount of $Ca_4Al_2(OH)_{14}$ that did not react with the chloride ions also reacted with $Al(OH)_4$ to generate $Ca_3Al_2(OH)_{12}$.

$$Ca_4Al_2(OH)_{14} + 2Cl^- \Rightarrow Ca_4Al_2Cl_2(OH)_{12}\downarrow + 2OH^- \quad (9)$$

$$3Ca_4Al_2Cl_2(OH)_{12} + 2Al(OH)_4^- + 4OH^- \Rightarrow 4Ca_3Al_2(OH)_{12}\downarrow + 6Cl^- \quad (10)$$

As the above chemical formula shows, too much $NaAlO_2$ will not improve the adsorption efficiency but will affect the adsorption. It is also essential to effectively control the appropriate ratio of CaO to $NaAlO_2$ to adsorb chloride ions. Mix-A and Sed-B can generate $Ca_4Al_2(OH)_{14}$ with a layered structure in sodium chloride solution. The substance that can effectively adsorb chloride ions in the whole system is $Ca_4Al_2(OH)_{14}$. The model of $Ca_4Al_2(OH)_{14}$ adsorbing chloride ions is shown in Fig. 10.

4. Conclusion

- The single factor experiment results show that under the same conditions, in 300 mg/L sodium chloride solution, the maximum adsorption efficiency of Sed-B is 16.67%, and the unit adsorption capacity is 4.45 mg/g. the maximum adsorption efficiency and unit adsorption mass of Mix-A for chloride ions were 80.0% and 20.81 mg/g, respectively. When the temperature is 25°C, the initial pH is 10, the stirring time is about 60 min, and the mass ratio of adsorbent is m($NaAlO_2$):m(CaO) = 1:2.5, Mix-A has the best adsorption effect on chloride ions. The adsorption efficiency can reach 93.3% in a 100 mg/L sodium chloride solution. With the increase of chloride concentration, the adsorption efficiency gradually decreases, but the unit adsorption mass gradually increases. When the concentration of sodium chloride is 2,000 mg/L, the unit adsorption mass can reach 63.50 mg/g at most.
- Adding CaO and $NaAlO_2$ to a sodium chloride solution can effectively adsorb chloride ions. The mechanism is that CaO and $NaAlO_2$ react in solution to generate a kind of $Ca_4Al_2(OH)_{14}$, which has a layered structure, and the OH^- between layers can carry out ion exchange with chloride ions in external solution. To form Friedel's salt ($Ca_4Al_2Cl_2(OH)_{12}$). Using this principle, excess chloride ions in wastewater can be effectively removed with low cost and simple method, which is beneficial to industrial applications and wastewater treatment. We believe that how to effectively prepare and extract $Ca_4Al_2(OH)_{14}$ also has further research significance, and it will have greater application to be used as chlorine absorbing filler in high chlorine environment.

Credit authorship contribution statement

Pengyu Zhang: Investigation, Writing-Original draft preparation, Limin Sun, Conceptualization, Supervision and Editing. Reviewing and Editing. Wenyang Li: Conceptualization, Supervision. Haomeng Guo: Conceptualization, Supervision, Ruian Gao: Investigation. Yong Guan: Supervision, Writing – reviewing & editing. Liming Feng: Funding acquisition, Writing – reviewing & editing.

Declaration of competing interest

The authors declare that they have no known competing financial interests or personal relationships that could have appeared to influence the work.

Acknowledgments

This work was financially supported by Central Government Guide Local Science and Technology Development Special Fund Project, YDZX2022112. and Shandong Province Science and Technology smes Innovation Ability Improvement Project, 2022TSGC1295.

References

[1] K.-F. Cao, Z. Chen, Y.-H. Wu, Y. Mao, Q. Shi, X.-W. Chen, Y. Bai, K.X. Li, H.-Y. Hu, The noteworthy chloride ions in reclaimed water: harmful effects, concentration levels and control strategies, Water Res., 215 (2022) 118271, doi: 10.1016/j.watres.2022.118271.

[2] J.H. Leng, Y. Frank Cheng, K.X. Liao, Y.J. Huang, F.L. Zhou, S. Zhao, X. Liu, Q. Zou, Synergistic effect of O_2-Cl^- on localized corrosion failure of L245N pipeline in CO_2-O_2-Cl^- environment, Eng. Fail. Anal., 138 (2022) 106332, doi: 10.1016/j.engfailanal.2022.106332.

[3] D.Q. Sun, Z. Zhou, Q. Ming, J.M. Guo, X.F. Ye, Y. Yuan, M.N. Zhang, X.D. Zhao, L.-m. Jiang, Q. Xia, Improving settleability and dewaterability of Friedel's salt for chloride removal from saline wastewater, Desalination, 509 (2021) 115070, doi: 10.1016/j.desal.2021.115070.

[4] E. Briz, M.V. Biezma, D.M. Bastidas, Stress corrosion cracking of new 2001 lean–duplex stainless-steel reinforcements in chloride contained concrete pore solution: an electrochemical study, Constr. Build. Mater., 192 (2018) 1–8.

[5] E.G. Stets, C.J. Lee, D.A. Lytle, M.R. Schock, Increasing chloride in rivers of the conterminous U.S. and linkages to potential corrosivity and lead action level exceedances in drinking water, Sci. Total Environ., 613–614 (2018) 1498–1509.

[6] C.Y. Yang, Pollution and prevention of chloride in surface water, Environ. Sustainable Dev., 1 (2004) 25–26.

[7] M.-H. Hong, S.-I. Pyun, Corrosive wear behaviour of 304-L stainless steel in 1 N H_2SO_4 solution part 2. Effect of chloride ion concentration, Wear, 147 (1991) 69–78.

[8] Q.-q. Wen, M.-c. Chen, Study on the nonlinear performance degradation of reinforced concrete beam under chloride ion corrosion, Eng. Fail. Anal., 124 (2021) 105310, doi: 10.1016/j.engfailanal.2021.105310.

[9] Z.W. Cui, G.R. Liu, C.H. Lu, *H.J. Wang,* Chloride ion erosion and durability life prediction of marine concrete beams under combined action of dry-wet cycle and flexural cracks, Bull. Chin. Ceram. Soc., 39 (2020) 344–351.

[10] X.-m. Zhang, Z.-y. Chen, H.-f. Luo, T. Zhou, Y.-l. Zhao, Z.-c. Ling, Corrosion resistances of metallic materials in environments containing chloride ions: a review, Trans. Nonferrous Met. Soc. China, 32 (2022) 377–410.

[11] Y.M. Li, Z.Z. Yang, K.H. Yang, J.J. Wei, Z.H. Li, C. Ma, X. Yang, T.T. Wang, G.M. Zeng, G.L. Yu, Z.G. Yu, C. Zhang, Removal

of chloride from water and wastewater: removal mechanisms and recent trends, Sci. Total Environ., 821 (2022) 153174, doi: 10.1016/j.scitotenv.2022.153174.
[12] J.M. Guo, Z. Zhou, Q. Ming, Z.J. Huang, J. Zhu, S. Zhang, J. Xu, J.F. Xi, Q.Q. Zhao, X.D. Zhao, Recovering precipitates from dechlorination process of saline wastewater as poly aluminum chloride, Chem. Eng. J., 427 (2022) 131612, doi: 10.1016/j.cej.2021.131612.
[13] X.F. Ye, X.D. Zhao, Q. Ming, J. Zhu, J.M. Guo, D.Q. Sun, S. Zhang, J. Xu, Z. Zhou, Process optimization to enhance utilization efficiency of precipitants for chloride removal from flue gas desulfurization wastewater via Friedel's salt precipitation, J. Environ. Manage., 299 (2021) 113682, doi: 10.1016/j.jenvman.2021.113682.
[14] D.Q. Sun, Z. Zhou, Q. Ming, J.M. Guo, X.F. Ye, Y. Yuan, M.N. Zhang, X.D. Zhao, L.M. Jiang, Q. Xia, Improving settleability and dewaterability of Friedel's salt for chloride removal from saline wastewater, Desalination, 509 (2021) 115070, doi: 10.1016/j.desal.2021.115070.
[15] X. Wang, S.Y. Lu, Z.L. Chen, Q.J. Mao, Study on the removal of chloride ion from the washing solution of municipal solid waste incineration fly ash, Acta Sci. Circ., 37 (2017) 2218–2222.
[16] P. Szczepański, H.P. Guo, K. Dzieszkowski, Z. Rafiński, A. Wolan, K. Fatyeyeva, J. Kujawa, W. Kujawski, New reactive ionic liquids as carriers in polymer inclusion membranes for transport and separation of Cd(II), Cu(II), Pb(II), and Zn(II) ions from chloride aqueous solutions, J. Membr. Sci., 638 (2021) 119674, doi: 10.1016/j.memsci.2021.119674.
[17] H. Chen, L.X. Zhan, L.Y. Gu, Q.Y. Feng, N. Zhao, Y.X. Feng, H. Wu, L.J. Yang, Chloride release characteristics of desulfurization wastewater droplet during evaporation process using the single droplet drying method, Fuel, 30 (2021) 121551, doi: 10.1016/j.fuel.2021.121551.
[18] R. Cherif, A. El Amine Hamami, A. Aït-Mokhtar, Global quantitative monitoring of the ion exchange balance in a chloride migration test on cementitious materials with mineral additions, Cem. Concr. Res., 138 (2020) 106240, doi: 10.1016/j.cemconres.2020.106240.
[19] L. Yang, L. Lv, S.J. Zhang, B.C. Pan, W.M. Zhang, Catalytic dechlorination of monochlorobenzene by Pd/Fe nanoparticles immobilized within a polymeric anion exchanger, Chem. Eng. J., 178 (2011) 161–167.
[20] W.Z. Liu, L. Lü, Y. Lu, X.W. Hu, B. Liang, Removal of chloride from simulated acidic wastewater in the zinc production, Chin. J. Chem. Eng., 27 (2019) 1037–1043.
[21] R. Hamidi, D. Kahforoushan, E. Fatehifar, The simultaneous removal of calcium, magnesium and chloride ions from industrial waste-water using magnesium-aluminum oxide, J. Environ. Sci. Health. Part A Toxic/Hazard. Subst. Environ. Eng., 48 (2013) 1225–1230.
[22] J. Dron, A. Dodi, Comparison of adsorption equilibrium models for the study of Cl^-, NO^{3-} and SO_4^{2-} removal from aqueous solutions by an anion exchange resin, J. Hazard. Mater., 190 (2011) 300–307.
[23] L. Lv, P. Sun, Z. Gu, H. Du, X. Pang, X. Tao, R. Xu, L. Xu, Journal of hazardous materials, removal of chloride ion from aqueous solution by ZnAl-NO_3 layered double hydroxides as anion-exchanger, J. Hazard. Mater., 161 (2009) 1444–1449.
[24] A. Abdel-Wahab, B. Batchelor, Chloride removal from recycled cooling water using ultra-high lime with aluminum process, Water Environ. Res., 74 (2002) 256–263.
[25] A. Abdel-Wahab, B. Batchelor, Effects of pH, temperature, and water quality on chloride removal with ultra-high lime with aluminum process, Water Environ. Res., 78 (2006) 930–937.
[26] Y. Xin, Z. Zhou, Q. Ming, D.Q. Sun, J. Han, X.F. Ye, S.F. Dai, L.M. Jiang, X.D. Zhao, Y. An, A two-stage desalination process for zero liquid discharge of flue gas desulfurization wastewater by chloride precipitation, J. Hazard. Mater., 397 (2020) 122744, doi: 10.1016/j.jhazmat.2020.122744.
[27] J.J. Zhang, H. Zhao, H.B. Cao, H.P. Li, Z.B. Li, Removal of Cd^{2+} from water by Friedel's salt (FS: $3CaO{\cdot}A1_2O_3{\cdot}CaCl_2{\cdot}10H_2O$): sorption characteristics and mechanisms, J. Environ. Sci., 25 (2013) 1719–1725.
[28] Y.C. Dai, G.R. Qian, Y.L. Cao, Y. Chi, Y.F. Xu, J.Z. Zhou, Q. Liu, Z.P. Xu, S.Z. Qiao, Effective removal and fixation of Cr(VI) from aqueous solution with Friedel's salt, J. Hazard. Mater., 170 (2019) 1086–1092.
[29] D. Li, X.Y. Guo, Q.H. Tian, Z.P. Xu, R.Z. Xu, L. Zhang, Synthesis and application of Friedel's salt in arsenic removal from caustic solution, Chem. Eng. J., 323 (2017) 304–311.
[30] Q.D. Yao, Analysis of the factors influencing the removal of chloride ion in leather wastewater by Friedel's salt method, Leather Chem., 38 (2021) 7–11.
[31] Z.L. Cheng, B.J. Yang, H.W. Tang, L.P. Hou, Experimental research on chloride removal from water by ultra-high lime with aluminum process, Ind. Water Treat., 35 (2015) 38–41.
[32] D.N. Zhang, Y.F. Jia, J.Y. Ma, Z.B. Li, Removal of arsenic from water by Friedel's salt (FS: $3CaO{\cdot}Al_2O_3{\cdot}CaCl_2{\cdot}10H_2O$), J. Hazard. Mater., 195 (2011) 398–404.
[33] C. Abate, B.E. Scheetz, Aqueous phase equilibria in the system CaO-Al_2O_3-$CaCl_2$-H_2O: the significance and stability of Friedel's salt, J. Am. Ceram. Soc., 78 (1995) 939–944.
[34] V.R.L. Constantino, T.J. Pinnavaia, Basic properties of $Mg_{2+1-x}Al_{3+x}$ layered double hydroxides intercalated by carbonate, hydroxide, chloride, and sulfate anions, Inorg. Chem., 26 (1995) 883–892.
[35] S.Y. Sui, M. Wu, Z.Q. Yang, F.J. Wang, Z.Y. Liu, J.Y. Jiang, An investigation on the formation of Friedel's salt in tricalcium silicate combined with metakaolin and limestone systems, Constr. Build. Mater., 284 (2021) 122855, doi: 10.1016/j.conbuildmat.2021.122855.
[36] L.J. Zhang, P. Lv, Y. He, S.W. Li, J.H. Peng, L.B. Zhang, K.H. Chen, S.H. Yin, Ultrasound-assisted cleaning chloride from wastewater using Friedel's salt precipitation, J. Hazard. Mater., 403 (2021) 123545, doi: 10.1016/j.jhazmat.2020.123545.
[37] Y. Shao, M. Zhou, W.X. Wang, H.B. Hou, Identification of chromate binding mechanisms in Friedel's salt, Constr. Build Mater., 48 (2013) 942–947.
[38] U.A. Birnin-Yauri, F.P. Glasser, Friedel's salt, $Ca_2Al(OH)_6(Cl,OH){\cdot}2H_2O$: its solid solutions and their role in chloride binding, Cem. Concr. Res., 28 (1998) 1713–1723.
[39] M.Y.A. Mollah, M. Kesmez, D.L. Cocke, An X-ray diffraction (XRD) and Fourier-transform infrared spectroscopic (FTIR) investigation of the long-term effect on the solidification/stabilization (S/S) of arsenic (V) in Portland cement, Sci. Total Environ., 325 (2004) 255–262.
[40] A.K. Suryavanshia, J.D. Scantleburyb, S.B. Lyonb, Mechanism of Friedel's salt formation in cements rich in tri-calcium aluminate, Cem. Concr. Res., 26 (1996) 717–727.